Title

Local Mechanical Perturbation Provides an Effective Means to Regulate the Growth and Assembly of Functional Peptide Fibrils

Journal

Small, 12(46)

ISSN

1613-6810

Authors

Karsai, Arpad
Slack, Teri Jo
Malekan, Hamed
et al.

Publication Date

2016-12-01

DOI

10.1002/smll.201601657

Peer reviewed

Local Mechanical Perturbation Provides an Effective Means to Regulate the Growth and Assembly of Functional Peptide Fibrils

*Arpad Karsai, Teri Jo Slack, Hamed Malekan, Fadi Khoury, Wei-Feng Lin, Victoria Tran, Daniel Cox, Michael Toney, Xi Chen, and Gang-yu Liu**

***M**ucin 1 (MUC1) peptide fused with Q11 (MUC1-Q11) having 35 residues has previously been shown to form amyloid fibrils. Using time-dependent and high-resolution atomic force microscopy (AFM) imaging, it is revealed that the formation of individual MUC1-Q11 fibrils entails nucleation and extension at both ends. This process can be altered by local mechanical perturbations using AFM probes. This work reports two specific perturbations and outcomes. First, by increasing load while maintaining tip-surface contact, the fibrils are cut during the scan due to shearing. Growth of fibrils occurs at the newly exposed termini, following similar mechanism of the MUC1-Q11 nucleation growth. As a result, branched fibrils are seen on the surface whose orientation and length can be controlled by the nuclei orientation and reaction time. In contrast to the "one-time-cut", fibrils can be continuously fragmented by modulation at sufficiently high amplitude. As a result, short and highly branched fibrils accumulate and pile on surfaces. Since the fibril formation and assembly of MUC1-Q11 can be impacted by local mechanical force, this approach offers a nonchemical and label-free means to control the presentation of MUC1 epitopes, and has promising application in MUC1 fibril-based immunotherapy.*

1. Introduction

MUC1-Q11 is a peptide of 35 residues comprising two distinct units linked via a spacer (SGSG) (**Figure 1**). It has a C-terminal self-assembly (QQKFQFQFQQQ) domain (Q11) and an N-terminal MUC1 peptide repeat (HGVTSAPDTRPAPGSTAPPA).[1,2] This peptide was initially designed for cancer immunotherapy applications.[2] Human MUC1 glycoproteins with abnormal O-glycans have been found in high abundance on surfaces of epithelial tumor cells and have been investigated as potential candidates for antitumor vaccines. Prior investigations suggest that the presentation of MUC1 directly impacts immunogenicity, e.g., MUC1 fibrils led to effective B-cell responses, while soluble monomeric MUC1 molecules exhibited little immunogenicity.[2,3] Therefore, the effective molecule is MUC1 conjugated with an eleven residue long Q11 peptide,[4] as shown in Figure 1. MUC1-Q11 molecules form amyloid fibrils that could present multiple epitopes on the surface, leading to effective activation of B-cells to produce anticancer antibodies.[2] While effective, the final presentation of fibrils depends on the interplay between self-assembly reaction kinetics and thermodynamics of the prior approaches. This work explores if the assembly of fibrils, ultimately the presentation of MUC1 or functional peptide units in general, could

Dr. A. Karsai, T. J. Slack, Dr. H. Malekan, F. Khoury, Dr. W.-F. Lin, V. Tran, Prof. M. Toney, Prof. X. Chen, Prof. G.-y. Liu
Department of Chemistry
University of California
Davis, CA 95616, USA
E-mail: gyliu@ucdavis.edu
Prof. D. Cox
Department of Physics
University of California
Davis, CA 95616, USA

DOI: 10.1002/smll.201601657

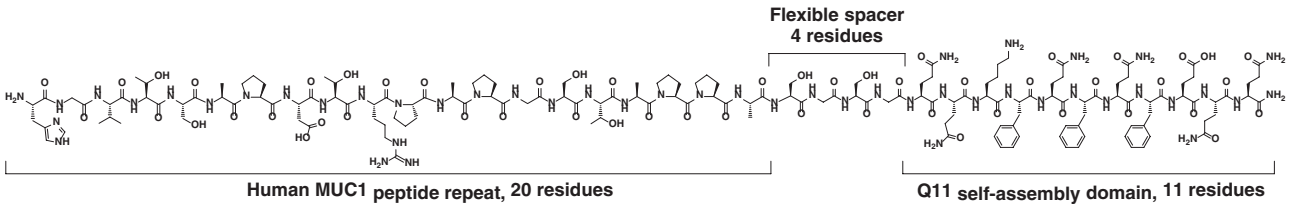

Figure 1. Primary sequence of MUC1-Q11.

be controlled to enable optimal presentations for desired biological applications.

For a protein with a given amino acid sequence, conventional means to regulate peptide and protein assembly include variations in temperature, concentration of peptide, and buffer conditions. These were effective in enabling assembly of long fibrils of peptides and proteins.[5–9] These methods rely on the interplay of kinetics and thermodynamics of peptide self-assembly reactions. The ultimate goal is to achieve programmable self-assembly to a designed length and spatial distribution. Toward this, and deviating from conventional means to regulate protein assembly, several attempts were reported on the use of surfaces to direct protein assembly, such as α-synuclein,[10] amyloid-like peptide,[11] Amyloid β(25-35),[9] and Amyloid β(25-35_N27C).[12] The mica(0001) surfaces, for example, facilitated the hexagonal arrangement of fibrils.[9–12] Another approach is to apply a local mechanical force to impact the nucleation and growth process of model amyloid proteins.[13,14] This approach was particularly effective for proteins consisting of silk-elastane-like blocks. These results brought us one step closer to controlling fibril growth, and triggered the following important questions: to what degree could this approach impact the fibril growth; and could this method be applied on biologically functional peptides?

Using MUC1-Q11 as a functional peptide system, this work demonstrates that local mechanical perturbation is an effective means to control the assembly of this protein. Atomic force microscopy (AFM) provides in situ mechanical perturbation as well as time-dependent structure characterization with nanometer resolution. The results indicate that the length and arrangement of the fibrils depend sensitively on the mechanical parameters. Local mechanical force provide a new means for researchers to regulate the peptide and protein self-assembly processes in order to produce designed building blocks for specific applications that include immunology, biomaterials construction and scaffold construction for tissue engineering, as well as construction of nanobiosensors.[5,15–17]

2. Results

2.1. Formation of MUC1-Q11 Fibrils on Surfaces as Monitored by Time-Dependent Imaging

Attachment of MUC1-Q11 to mica, as well as its fibril growth, was monitored in a liquid cell by time-dependent imaging using atomic force microscopy. Typically, a freshly cleaved mica(0001) surface was exposed to 10×10^{-6} M of MUC1-Q11 solution at room temperature, and a 1.5 μm x 1.5 μm region was imaged every 5 min. From time to time, we zoomed into the designated region to visualize specific fibril growth in detail. **Figure 2** (top row) shows two snapshots selected from the 1.5 μm x 1.5 μm scans at various times showing characteristic growth behavior of MUC1-Q11 on mica surfaces: protein attaches to surfaces to form nucleation sites during the first few minutes, then these nucleation sites grow into fibrils over time. The imaging rate was 1.95 Hz, imaging time of a single frame was 4 min 20 s. The growth rate from each nucleation site varies and ranges from 7 to 13 nm min^{-1}. As a result, the fibrils become longer and the surface coverage increases with time. Increasing protein concentration resulted in high fibril coverage (Figure 2C). At 100×10^{-6} M concentration, fibrils formed within a few minutes and fibrils formed multiple layers stacked on each other. Nanoshaving[18] revealed that there are three layers of fibrils that can be distinguished (data not shown).

Figure 2D,E also show high-resolution imaging of three characteristic growths of fibrils 1–3. Fibril 1 represents the complex nucleation dependent growth behavior of MUC1-Q11 fibrils: i.e., the nucleus is formed within the first few minutes. The nucleus measures 20 nm in length and is 2.0–2.5 nm in height, which is consistent with the short oligomers of MUC1-Q11. Following the nucleation, linear elongation was observed on one end of the fibril at a rate of 6.7 nm min^{-1} in the first 45 min. The elongating fibril exhibited sudden burst-like elongation steps and minutes long slow growing periods. The elongation slowed down after 45 min and stopped when the fibril reached another fibril. Fibril 2 elongated at both ends with a growth rate of 8.67 nm min^{-1} in the first 35 min. In fibril 2, the nucleus formed within the first 15 min, then the fibril started to extend. The growth rate was linear up to 35 min, then slowed down as the top end came in close proximity to fibril 3. The elongation stopped for 25 min without any obvious reason when the fibril reached 290 nm in length. Fibril 3 followed a similar trajectory as fibril 2, with a faster, 10 nm min^{-1} elongation rate (see Figure 2E,F). Carefully following all sites shown in Figure 2, the variations in fibril growth include: (a) the majority of fibrils following linear growth at both ends at an initial rate in the first 30–60 min; (b) some fibrils only extend at one end; (c) growth rate, in some cases, changes with time leading to variation in slope of the length versus time plots; (d) growth terminates when the ends hits an impediment such as another fibril or protein aggregate. Occasionally, growth halts for no obvious reason. The experiments were repeated three times using 10×10^{-6} M peptide concentrations. In all cases we found that MUC1-Q11 fibrils

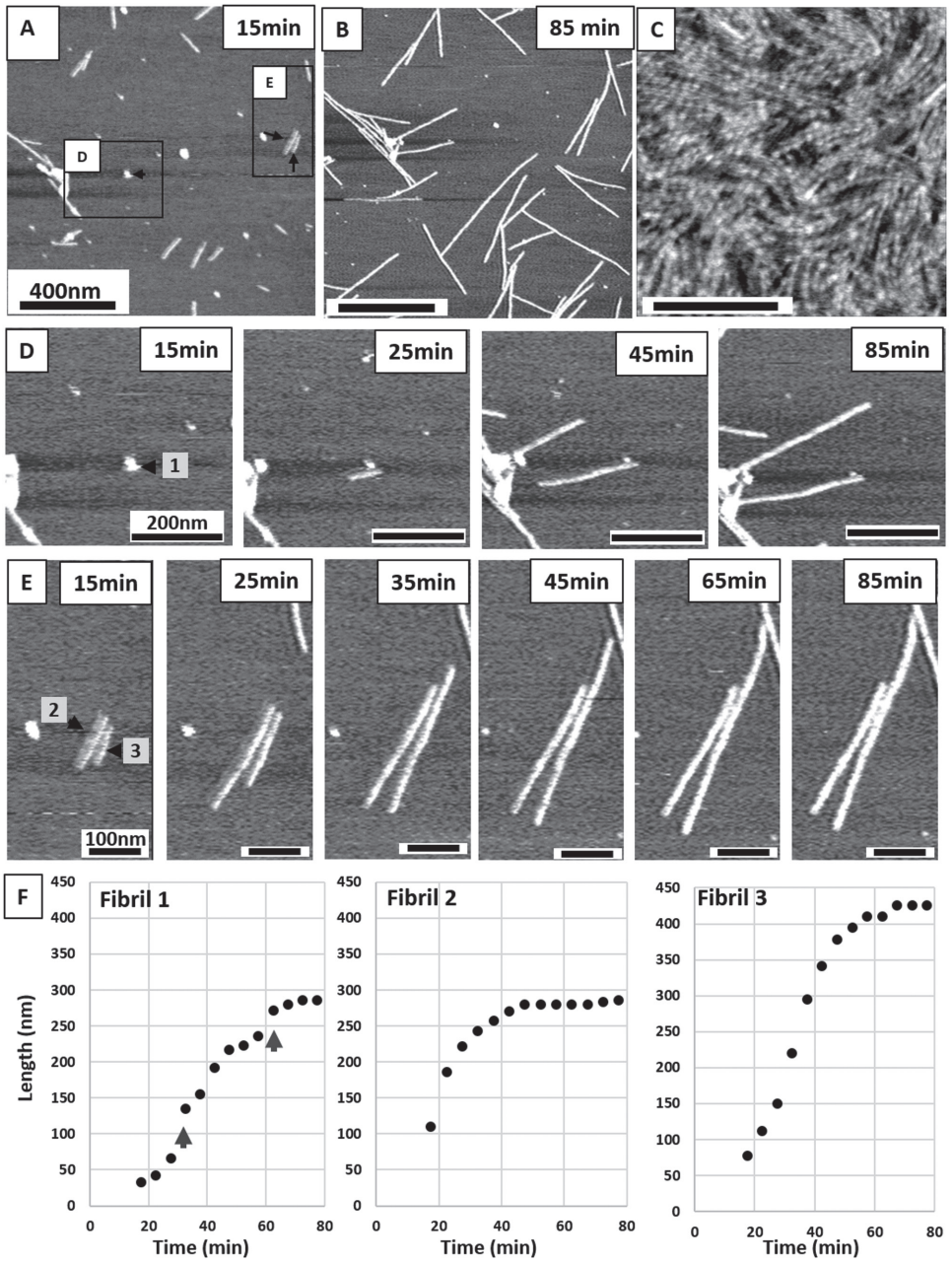

Figure 2. A) Tapping mode image of MUC1-Q11 fibrils on a mica surface 15 min after deposition of a 10×10^{-6} M solution. Black rectangles indicate the zoom areas which are shown in panels (D) and (E). The numbers and arrows indicate three representative fibrils with elongation rate plotted in the bottom panel. B) Snapshot image of the same area 85 min after sample deposition. C) Tapping mode image of packed fibrils at high 100×10^{-6} M peptide concentration. D) High resolution time-lapse AFM images of MUC1-Q11 fibril 1. E) Time-lapse images of two elongating fibrils: Fibrils 2 and 3. F) Length versus time plots of Fibrils 1–3. Arrows on the first graph indicate the sudden burst-like elongation steps of Fibril 1.

form a similar stable network on the mica surface within 60–90 min. Detailed, single fibril level analysis was carried out for the presented data set.

These behaviors are similar to previous observations of Amyloid β(25-35). Amyloid β(25-35) forms linear fibrils that are 1–4 nm tall, and several hundred nanometers long on a mica(0001) surface. The fibrils exhibit both fast and slow growing ends and step-wise assembly kinetics with burst-like elongation steps and pauses, similar to that observed with MUC1-Q11.[19] These observations and growth rates for MUC1-Q11 on mica(0001) serve as a good reference to compare growth under the same reaction conditions but with mechanical perturbations.

2.2. The Assembly of MUC1-Q11 Molecules on Surfaces can be Altered by Shearing the Newly Formed Fibers into Smaller Segments

Mechanical perturbation of MUC1-Q11 assembly on mica surfaces is illustrated in **Figure 3**. Under the same reaction condition as that in Figure 2, MUC1-Q11 molecules formed

www.MaterialsViews.com

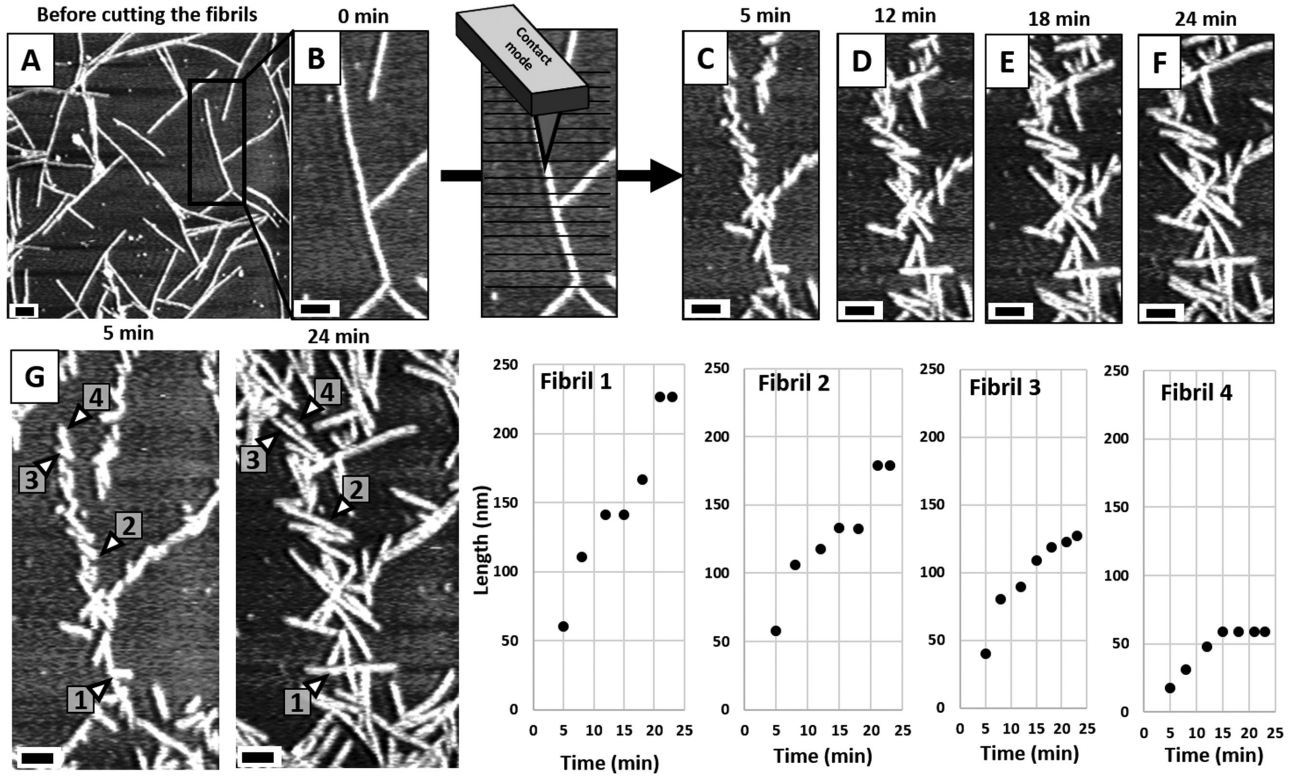

Figure 3. Effect of contact mode mechanical perturbation on MUC1-Q11 fibrils. A) Fully grown MUC1-Q11 fibrils on mica surface. Rectangle indicates one single fibril, which is shown in the rest of the figure. B) Selected fibril prior to cutting. Schematic shows the experimental setup. Horizontal black lines indicate the cut lines, which had 23 nm separations in the experiment. C) Image at 5 min time point shows the fragmented fibril after contact mode cutting. The lateral force of the cantilever dislocated the small fibril segments, which started growing immediately. D–F) Time-lapse images show the elongation of new fibrils. G) Panel highlights four representative fibrils and their growth kinetics. Each scale bar = 100 nm.

fibrils on mica(0001) surfaces within 90 min. Typical fibrils at that stage of the reaction measured 1.5–2.0 nm tall, with lengths ranging 100–800 nm with little bending. The elongation significantly diminished after 90 min exposure, and fibrils were immobilized on mica as shown in Figure 3A. Increasing the contact force or load to 1.0 nN, the AFM tip made parallel lines with a spacing of 23 nm. Due to the high shear force, the fibrils were cut into smaller segments during the scan, the lengths of which depended on the orientation of the original fibril with respect to the scanning direction. In the case shown in Figure 3, 20–100 nm segments were attained during the high force scan. The behaviors of newly formed segments were then monitored under tapping mode imaging as a function of time.

Zooming in to one fibril that is ≈75° to the cutting direction, time-dependent imaging reveals growth in detail, as shown in Figure 3C–F. The imaging rate was 3 Hz, and imaging time of a single frame was 2 min 50 s in Figure 3C–F. The newly cut segments were oriented in a zig-zag fashion along the initial fibril direction, which is to be expected considering the back and forth scan. Within minutes, the extensions at both ends were clearly visible and new fibrils grew with time. These observations suggest that the segments serve as nucleation sites for the growth of new MUC1-Q11 fibrils, following similar nucleation growth pathways as the initial fibril formation. The time-dependent growth is analyzed by plotting length versus time for each new fibril, of which four examples are shown in Figure 3 (bottom). The growth rate varies from segment to segment, and measures 4.1–8.5 nm min^{-1}. Similar to the initial formation of MUC1-Q11 fibrils on mica, these new fibrils exhibit variations in growth profile, such as (a) steady linear growth (8.5 nm min^{-1} interrupted by 3–5 min pauses (Fibril 1); (b) linear growth mingled with minute-long pause and rapid elongation step (20 nm min^{-1}) (Fibril 2); (c) linear growth followed by slowed growth kinetics (Fibril 3); (d) fibril elongation stops after linear growth period (Fibril 4.). These new growths reach saturation at 15 to 20 min, with fibril lengths ranging from 60 to 225 nm. MUC1-Q11 forms a stable fibril network on mica surface. The cutting does not cause the dissociation of the fibrils. However, the mechanical perturbation dislocates the cut sites from their original orientation. This suggests that MUC1-Q11 fibrils have a high affinity for the mica surface and can withstand partial dissociation and lateral shifts probably due to multiple flexible binding sites between charged peptide monomers and the mica surface.

To verify that the observations are caused by local mechanical perturbation instead of artifacts, we zoomed out of the perturbed area and compared the uncut region with the cut area, in situ. **Figure 4**D is a snap shot acquired 30 min after cutting, where the difference between the cut (central) and uncut (surrounding) areas are clearly visible. The fragmentation and new fibril growth is very consistent throughout the perturbed 1.5 μm × 1.5 μm region, as can

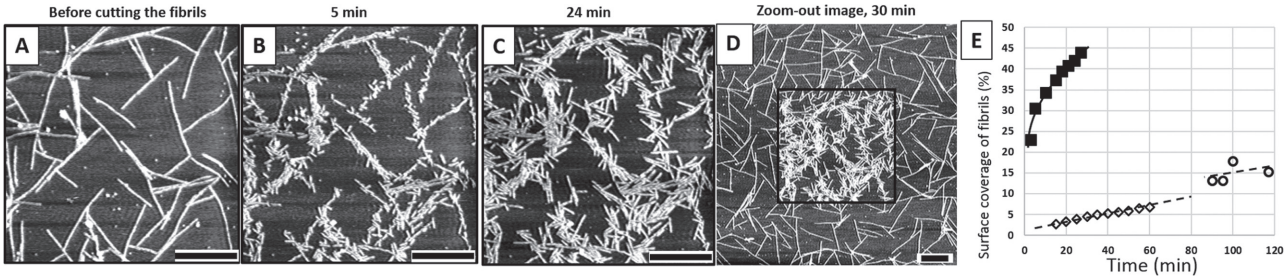

Figure 4. A) MUC1-Q11 fibrils prior to mechanical perturbation. B) Small fibril nuclei after mechanical perturbation. C) The small fibril fragments keep elongating on the mica surface forming a high density patch of fibrils. D) The zoom-out image clearly shows that fibril elongation happened only on the area where fibrils were subject to mechanical perturbation. E) Surface coverage of fibrils before and after the mechanical perturbation. Empty diamonds indicate the time-dependent increase of surface coverage of the control sample, which increases up to 7% in 60 min. Empty circles indicate the increase of fibril coverage of the control sample up to 120 min. Rectangles show the effect of mechanical cutting on fibril coverage. Each scale bar = 400 nm.

be seen from Figure 4B,C compared to Figure 4A. Coverage in both areas are plotted and compared in Figure 4E, where the perturbed area contains more, although shorter, fibrils than those in the surrounding areas. The kinetics of apparent fibril coverage after contact mode cutting shows that it is limited by the number of initial nuclei and the individual growth behavior of single fibrils. After the initial 10 min fast growing phase, the surface coverage increases from 12% to 35%. Afterward, the fibril elongation and the rate of surface coverage slow down. The coverage reaches 42% after 27 min.

The fact that both naturally growing and newly generated termini can stop elongating without any obvious reason suggests that growing fibrils are susceptible to kinetic traps. These could either be a stable conformation that is incompatible with elongation of fibrils or an extension inhibitor bound to the terminus. The sudden burst-like elongation of fibrils is similar to the growth behavior of Amyloid β(25-35).[19] It is possible that the elongating end of MUC1-Q11 fibrils fluctuate between two different conformations: a blocked state and a growing state similar to what was proposed to explain the growth kinetics of Amyloid β(25-35).[19] A previous study proved that protonated amino groups are responsible for attaching Amyloid β(25-35) fibrils to the potassium binding sites of the mica surface.[9] Similarities between the elongation kinetics of single MUC1-Q11 fibrils and Amyloid β(25-35) fibrils on mica suggest that MUC1-Q11 fibrils can have comparable interactions via its Lysine residues and amino termini. These positively charged sites can provide flexible binding and maintain strong affinity of MUC1-Q11 nuclei and fibrils in multiple different orientations on mica surface. These binding properties of MUC1-Q11 are probably the key features of the system which allow the use of mechanical force in situ to manipulate and control fibril growth without facilitating their dissociation from the substrate.

Taken collectively from Figures 3 and 4, the cutting of MUC1-Q11 fibrils produces smaller segments 20 to 100 nm in length. These segments serve as new nucleation sites from which fibrils grow, similar to Amyloid β(25-35) peptides.[19] The net result is an increase in nucleation sites on surfaces, redirection of fibril orientation, and increased surface coverage.

2.3. Lengths and Numbers of New Nuclei can be Accurately Defined

We can predetermine the number of new fragments and their lengths by line density and the azimuthal angle of the cutting with respect to orientation of the fibrils. The relationship between the orientation of the fibril and the density of cutting lines can be described with the following equation: length of new fragments = cut line spacing/sin α, where α is the angle between the fibril and the cutting lines, as it is described in **Figure 5**. The figure shows three different scenarios at 23 nm cutting line spacing. Figure 5A shows a 278 nm long fibril, 73° crossing the scan. Cutting this fibril should result in 11 fragments with lengths of 24 nm. In reality, we attained 6 fibrils 22 ± 4 nm in length, and another 5 fibrils twice as long. The longer, 44.9 ± 4 nm fibrils are due to the elongation of fibrils which took place in ≈4 min time frame, after cutting but before the image was taken.

Figure 5B shows a 274 nm long fibril that is 38° from the cut line. Post cutting yielded six new nuclei 48 ± 12 nm, and one fragment of 104 nm. The predicted length and number of fibrils are 37 nm and 7, respectively. The results follow the anticipated value with only one cutting point failing to break the bond. Figure 5C shows a 275 nm fibril almost parallel (4°) to the scan. In this scenario the cutting is a rare event, as it is supposed to happen once in every 333 nm along the fibril. The image shows that there is a single, 22 nm long fragment cut off from the original fibril. This result indicates that a single cut can remove short fragments from the fibrils.

2.4. Continuous Cutting Leads to Responding Growth and Reassembly of Fibrils

To explore the effect of various mechanical perturbations and the versatility of the system, we modulate the normal force via tapping mode signal, as illustrated in **Figure 6**. The normal force can be regulated by setting the damping magnitude (in %): low damping is suitable for tapping-mode imaging, while high damping could lead to cutting of fibrils due to transient and local pressure. Figure 6A shows mica surface with a low density of MUC1-Q11 fibrils 15 min after soaking in protein solution. By damping at 40% of initial amplitude,

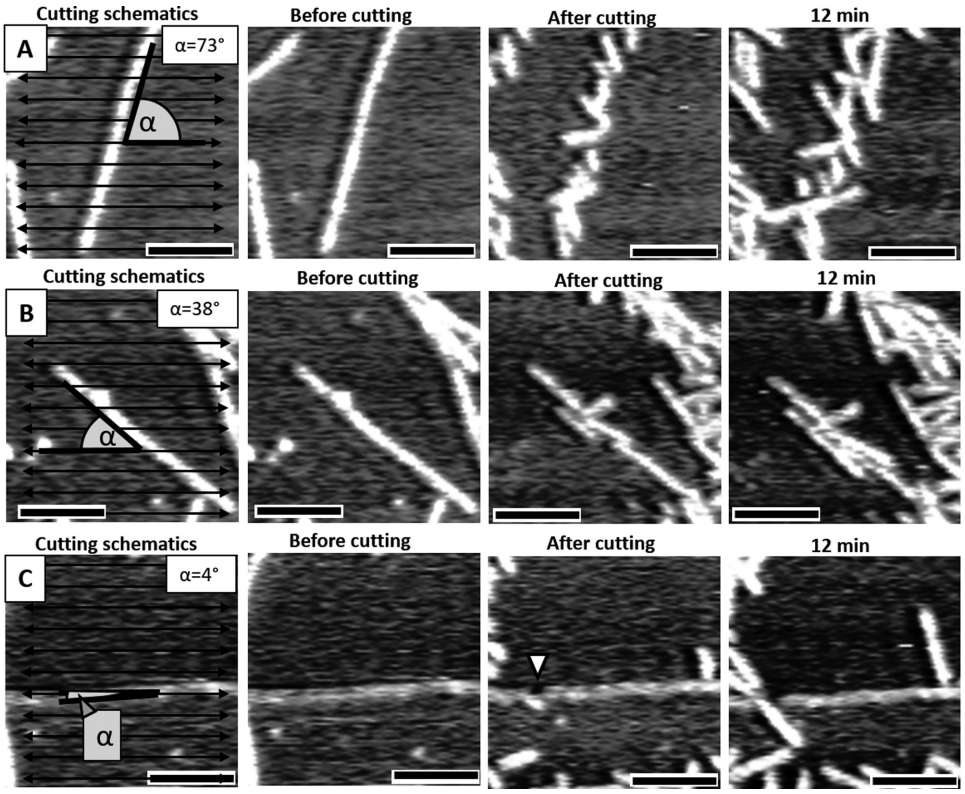

Figure 5. AFM images to reveal the fragments produced after high force scan via AFM probe. Each row reveals AFM topographs of one fiber before, and after, cutting. The fibril is orientated by 73°, 38°, and 4° respectively from top to bottom. Scale bar = 100 nm.

these initial fibrils were subjected to tapped and continuous cutting. Images taken 5 min after the first cut revealed segmentation of fibrils, and some branching. Repeated cutting led to dramatic changes, as shown in Figure 6C, where high-density and short fibrils appear. The number and positions seem to be constant with the formation of new nuclei and growth, similar to that shown in Figure 3. The difference is the tapped and continuous cut in Figure 6, in contrast to one-time sheering in Figure 3. As a result, a much higher number of nuclei were formed, leading to high density fibril patches with fibril lengths ranging from 50 to 150 nm (Figure 5D).

To verify that the mechanical perturbation was the cause of fibril reassembly, we compared the mechanically perturbed area with its surrounding, as shown in **Figure 7**. In the perturbed area, time-dependent growth of fibril was evident, as shown by the three snapshots shown in Figure 7A–C. Tapping and continuous cutting resulted in new fragments in each cycle, and as such, some of the newly formed fibrils were also fragmented, serving as new sites for growth and assembly. This led to a more rapid increase of surface coverage as shown in Figure 7E, where the coverage increased exponentially with time, from 12% to 73% in 50 min. The

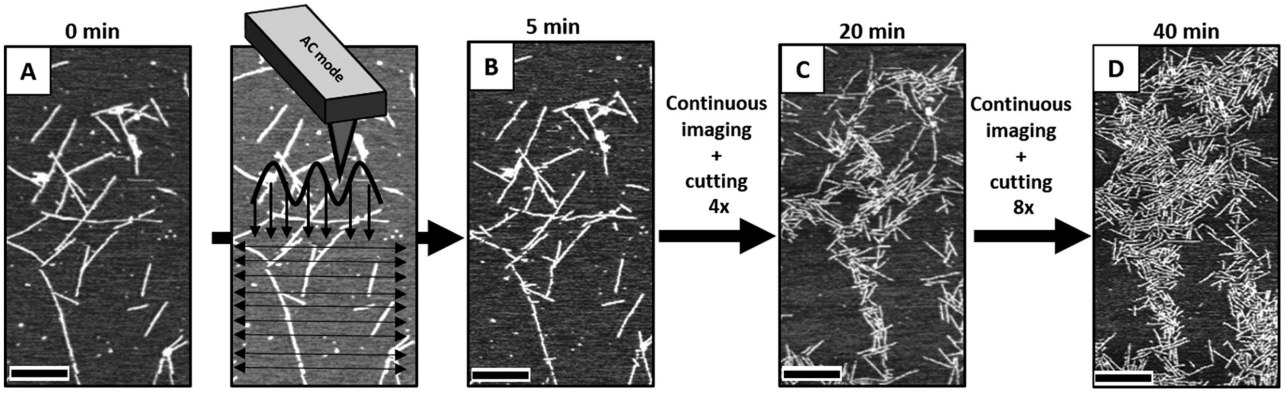

Figure 6. A) MUC1-Q11 fibrils on mica(0001) imaged 15 min after soaking in protein solution. We define this image as time zero, at which high damping was applied to cut the fibrils. The image beside (A) is a duplication of image (A) with a schematic diagram to illustrate the tapped and continuous cutting. The spacing of scanning lines is 2.93 nm. B) The same area as (A) imaged 5 min after the first cutting. C) The same area as (A) after four repeated perturbations via tapped and continuous cut, acquired 20 min after image (A). D) The same area as (A) after eight repeated perturbations via tapped and continuous cut, acquired 40 min after image (A). Each scale bar = 400 nm.

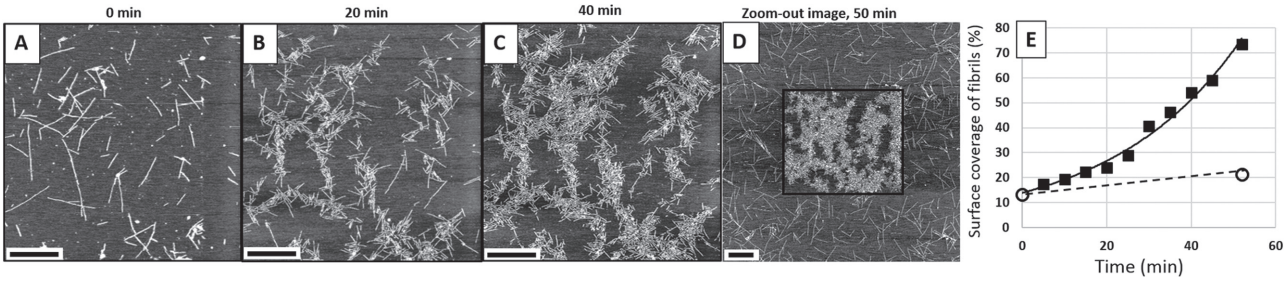

Figure 7. A) A 2000 nm × 2000 nm AFM topograph of MUC1-Q11 fibrils on mica(0001) surface, after depositing protein solution on mica for 15 min. We define this image as time zero, at which high damping was applied to cut the fibrils. Imaging times of single frames were 5 min. B) The same area after eight repeated cutting via tapping at 60% damping, acquired 20 min after image (A). C) The same area after 32 cutting cycles. D) A zoom-out view containing the perturbed area to allow for a side-by-side comparison in situ. E) Time-dependent surface coverage of the mechanically perturbed area (black rectangles) and its surrounding region (open circles). Scale bar = 400 nm.

fibrils were shorter and with a more narrow length distribution than were the initial fibrils as well as the fibrils grown in the experiments shown in Figure 3. The zoom-out image clearly shows that increased fibril growth happened only in the area subject to mechanical perturbation (Figure 7D). The coverage in the control area only reached 21% after a much longer time (50 + 15 min). In the case of one-time sheering (Figure 3), new fragments were generated, each having two freshly exposed ends to initiate the growth and reassembly of fibrils, which ultimately led to longer fibrils than shown in Figure 7D, under the same reaction time.

Our observations are similar to those observed for EAK16-II peptides reported previously.[14] In the case of EAK16-II peptides, the new fibril growth was consistent with reassembly at both ends. Analogous perturbation was also applied to silk-elastane-like nanofibers, from which patterns of fibril can be formed on mica(0001) surfaces.[13] The significance of our finding is the fact that MUC1-Q11 carries a specific biological functionality, i.e., the MUC1 unit for activation of antitumor B-cell response.[1,2] Therefore, the new growth and reassembly by local mechanic means offer a promising platform to impact immune responses.

3. Discussion

The presentation of MUC1 epitope to B-cells is crucial for proper antitumor immune response.[2] MUC1 monomers need to have a highly ordered structure and arrangement within the longitudinal axis of MUC1-Q11 fibrils in order to be recognized by B-cells. In a previous study,[2] the interactions between MUC1-Q11 fibrils with B-cells were random. The fibrils were dispersed in solution and therefore orientation and frequency of their interaction with cells were limited by the diffusion of fibrils and their encounters with cells. It is also known that rational design and spatial arrangement of molecules at the nanometer scale are highly effective for triggering and/or controlling cellular responses.[20,21] By controlling MUC1-Q11 fibrils on mica surfaces, the functional units are arranged in a more defined way than in solution phase, which could impact or even facilitate more pronounced B-cell responses and production of higher titer of anticancer antigens. Moreover, using local mechanical perturbations to impact biologically relevant fibril assembly at a nanometer level provides a new platform to engineer new hierarchical structures of self-assembling peptides and proteins, and therefore offers great promise to understand and control self-assembly of protein fibrils in order to produce new biomaterials, as well as to improve amyloid-based immunotherapy.

4. Conclusions

Using AFM and MUC1-Q11 fibril formation on mica(0001) surfaces, we have successfully demonstrated that the growth and assembly of fibrils can be impacted by local mechanical perturbation, e.g., cutting of fibrils. When sheering the MUC1-Q11 fibrils under high load, AFM probes fragment fibrils underneath. The length of fragments is defined by the line density of the scanning line, and the fibril orientation with respect to the scan. The two ends in each fragment become new nuclei, where new fibril grow or are extended. The distribution and surface coverage of the resulting fibrils are dictated by the cutting sites, and time of growth and initial fibril locations. When applying tapped force with sufficiently high transient pressure, the original and newly assembled fibrils were cut at the tip-fibril contact. As a result, a high number of nucleation sites were created which led to a large amount of surface bound short fibrils. The arrangements of these fibrils can be impacted by the cutting sites, number of repeated scans, as well as the protein solution concentration and reaction time. These observations are significant because the growth and assembly of functional peptide fibrils can be regulated via local mechanical perturbation. These results can be harnessed to produce designed assemblies of fibrils to elicit responses of B-cells, or form patterns on surfaces to enable construction of functional biomaterials.

5. Experimental Section

Materials: Materials and reagents used for peptide synthesis were purchased from AAPPTec (Louisville, Kentucky, U.S.A.) and used without further purification unless otherwise noted.

Specifically, the following materials were acquired: Rink Amide high yield resin, dimethylformamide (DMF), Fmoc protected amino acid, (1-Cyano-2-ethoxy-2-oxoethylidenaminooxy)dimethylamino-morpholino-carbenium-hexafluorophosphate (COMU) coupling reagent, and N,N-Diisopropylethylamine (DIEA), piperidine, cleavage cocktail trifluoroacetic acid (TFA): triisopropylsilyl ether (TIPS):H_2O (95:2.5:2.5) by volume.

The HPLC column used for purification was a reverse phase semipreparative Phenomenex Jupiter 10 μm C18 250 × 21.2 mm (Phenomenex, Torrance, CA, U.S.A.). RP-HPLC was performed on a Shimadzu instrument (Shimadzu Corp., Kyoto, Japan) comprised of dual pumps (Shimadzu LC-6AD), system controller (Shimadzu SCL-10A VP), automatic injector (Shimadzu SIL-10AP), photodiode array detector (Shimadzu SPD-M20A), and fraction collector (Shimadzu FRC-10A). UV detection was at 214 nm and a linear gradient of acetonitrile (ACN) and H_2O (0.1% trifluoroacetic acid) from ACN 0% to 50% ACN over 50 min with 10 mL min^{-1} flow rate. Mass spectra were recorded on a Bruker UltrafleXtreme MALDI-TOF/TOF Analyzer (Bruker, Billerica, Massachusetts, U.S.A.). Phosphate buffered saline (PBS) was purchased from Corning (VA, U.S.A.). The mica was purchased from Ted Pella Inc (CA, U.S.A.).

Synthesis of MUC1-Q11 Peptide: The synthesis of the MUC1-Q11 peptide (His-Gly-Val-Thr-Ser-Ala-Pro-Asp-Thr-Arg-Pro-Ala-Pro-Gly-Ser-Thr-Ala-Pro-Pro-Ala-Ser-Gly-Ser-Gly-Gln-Gln-Lys-Phe-Gln-Phe-Gln-Phe-Glu-Gln-Gln-NH_2) was performed as described.[22] Briefly, 10 mL polypropylene tube fit with a polyethylene porous disk using standard solid phase peptide synthesis (SPPS) on Rink Amide high yield resin (100 mg; loading = 0.45 mmol g^{-1}). The beads were swollen in DMF for 1 h prior to coupling. Building the peptide from the C-terminus to the N-terminus, each peptide bond formation was carried out with 5 eq. of the Fmoc protected amino acid, 5 eq. of COMU coupling reagent, and 10 eq. of DIEA in DMF. The reaction was mixed constantly at room temperature for 30–60 min and monitored by a Kaiser test. The beads were washed with DMF (3×), methanol (3×), and DMF (3×) after coupling. The washes were removed by suction. Each N-terminus Fmoc deprotection was achieved with 1:4 piperidine:DMF and mixed constantly for 30 min at room temperature. Beads were washed with DMF (6×) after deprotection. The peptide was cleaved from the bead using the cleavage cocktail TFA:TIPS:H_2O (95:2.5:2.5) by volume. The TFA was evaporated and cold diethyl ether was added to precipitate the peptide. The solution was centrifuged at 4000 rpm at 4 °C for 10 min and decanted (3× in cold ether). The crude peptide was dried and dissolved in water for reverse-phase HPLC purification (ACN/H_2O) to give the pure product as a fluffy white powder (42% yield) (Figure S1, Supporting Information). MS (MALDI-TOF/TOF) m/z $[M+H]^+$ Calcd. for $C_{158}H_{238}N_{48}O_{52}$ 3640.749; found $[M+H]^+$ 3640.666 (Figure S2, Supporting Information).

Preparation of MUC1-Q11 Solutions: Lyophilized MUC1-Q11 was dissolved in diluted sterile PBS buffers (pH 7.4, Corning, VA, U.S.A., 1/6 of original concentration, with 23.3×10^{-3} M NaCl) to reach a final peptide concentration of 400×10^{-6} M. To facilitate the dissolution of peptide, the mixture was pipetted up and down several times and vortexed for 30 s. The solution was stored at room temperature for 24 h to allow thorough mixing. For AFM imaging, the solution was diluted 20–40 times with ultra-pure MilliQ water to reach the 10×10^{-6} to 20×10^{-6} M final concentration. A 100–150 μL of the newly diluted MUC1-Q11 solution was introduced into AFM liquid cell containing a freshly cleaved mica(0001) surface to allow time-dependent investigation.

AFM Imaging: Images were taken with MFP3D-Bio AFM (Oxford Instrument, Santa Barbara, California, U.S.A.) using a Biolever-A cantilever (k = 30 pN nm^{-1}, Olympus, U.S.A.) in tapping mode. The driving frequency was in resonance with the fundamental vibration of the cantilever, typically between 9 and 10 kHz in water. Images were acquired at speeds of 7.5 or 11.27 μm s^{-1}, with 1024 × 512 pixels per frame. Both data acquisition and basic analyses were executed using MFP-3D software developed based on the Igor Pro 6.12 platform. Fibril length was measured by using ImageJ software (NIH). To study the time-dependent growth of fibrils, gentle tapping conditions were used to avoid cutting fibrils, e.g., 20% damping of vibrational amplitude. AFM imaging started immediately after injection of peptide solution to AFM liquid cell containing designated surfaces. Images were continuously taken. The time required to complete one image varied between 3 and 5 min, depending on the scan size and scan speed. The image times of presented experiments are indicated in Section 2. Typically, 10 to 15 images were acquired to allow monitoring of time-dependent investigations. The spring constant of cantilever was determined before mechanical perturbation experiments. To calibrate the cantilevers we used the thermal noise method[23] and the built-in software of our Asylum Research MFP3D instrument.

Supporting Information

Supporting Information is available from the Wiley Online Library or from the author.

Acknowledgements

This work was supported by the UC-Davis Campus Research Investments in Science and Engineering (RISE) program from the UC Davis Office of Research and NSFCHE-14137087. Some AFM images were acquired using the instrument at Keck Spectral Imaging Facility initiated by NSF-MRI and subsequently upgraded under the support of W. M. Keck Foundation.

[1] K. Pillai, M. H. Pourgholami, T. C. Chua, D. L. Morris, *Am. J. Clin. Oncol.* **2015**, *38*, 108.
[2] Z.-H. Huang, L. Shi, J.-W. Ma, Z.-Y. Sun, H. Cai, Y.-X. Chen, Y.-F. Zhao, Y.-M. Li, *J. Am. Chem. Soc.* **2012**, *134*, 8730.
[3] Z.-H. Huang, Z.-Y. Sun, Y. Gao, P.-G. Chen, Y.-F. Liu, Y.-X. Chen, Y.-M. Li, *Vaccines* **2014**, *2*, 549.
[4] J. S. Rudra, T. Sun, K. C. Bird, M. D. Daniels, J. Z. Gasiorowski, A. S. Chong, J. H. Collier, *ACS Nano* **2012**, *6*, 1557.
[5] M. D. Peralta, A. Karsai, A. Ngo, C. Sierra, K. T. Fong, N. R. Hayre, N. Mirzaee, K. M. Ravikumar, A. J. Kluber, X. Chen, G. Y. Liu, M. D. Toney, R. R. Singh, D. L. Cox, *ACS Nano* **2015**, *9*, 449.
[6] S. D. Solares, J. Chang, J. Seog, A. U. Kareem, *J. Appl. Phys.* **2011**, *110*, 094904.

[7] X. Zhou, Y. Zhang, F. Zhang, S. Pillai, J. Liu, R. Li, B. Dai, B. Li, Y. Zhang, *Nanoscale* **2013**, *5*, 4816.
[8] S. Jun, Y. Hong, H. Imamura, B. Y. Ha, J. Bechhoefer, P. Chen, *Biophys. J.* **2004**, *87*, 1249.
[9] A. Karsai, L. Grama, U. Murvai, K. Soos, B. Penke, M. S. Z. Kellermayer, *Nanotechnology* **2007**, *18*, 345102.
[10] W. Hoyer, D. Cherny, V. Subramaniam, T. M. Jovin, *J. Mol. Biol.* **2004**, *340*, 127.
[11] S. G. Kang, H. Li, T. Huynh, F. Zhang, Z. Xia, Y. Zhang, R. Zhou, *ACS Nano* **2012**, *6*, 9276.
[12] A. Karsai, U. Murvai, K. Soos, B. Penke, M. S. Kellermayer, *Eur. Biophys. J.* **2008**, *37*, 1133.
[13] J. Chang, X. F. Peng, K. Hijji, J. Cappello, H. Ghandehari, S. D. Solares, J. Seog, *J. Am. Chem. Soc.* **2011**, *133*, 1745.
[14] H. Yang, S. Y. Fung, M. Pritzker, P. Chen, *Angew. Chem. Int. Ed.* **2008**, *47*, 4397.
[15] C. A. Hauser, S. Maurer-Stroh, I. C. Martins, *Chem. Soc. Rev.* **2014**, *43*, 5326.
[16] N. Stephanopoulos, J. H. Ortony, S. I. Stupp, *Acta Mater.* **2013**, *61*, 912.
[17] S. Kyle, A. Aggeli, E. Ingham, M. J. McPherson, *Trends Biotechnol.* **2009**, *27*, 423.
[18] S. Xu, G. Y. Liu, *Langmuir* **1997**, *13*, 127.
[19] M. S. Z. Kellermayer, A. Karsai, M. Benke, K. Soos, B. Penke, *Proc. Natl. Acad. Sci. USA* **2008**, *105*, 141.
[20] Z. Deng, I. C. Weng, J. R. Li, H. Y. Chen, F. T. Liu, G. Y. Liu, *ACS Nano* **2011**, *5*, 8672.
[21] J. R. Li, S. S. Ross, Y. Liu, Y. X. Liu, K. H. Wang, H. Y. Chen, F. T. Liu, T. A. Laurence, G. Y. Liu, *ACS Nano* **2015**, *9*, 6738.
[22] H. Malekan, G. Fung, V. Thon, Z. Khedri, H. Yu, J. Qu, Y. Li, L. Ding, K. S. Lam, X. Chen, *Bioorg. Med. Chem.* **2013**, *21*, 4778.
[23] J. L. Hutter, J. Bechhoefer, *Rev. Sci. Instrum.* **1993**, *64*, 1868.

Received: May 16, 2016
Revised: June 30, 2016
Published online: September 30, 2016